In Situ Intercalation Replacement and Selective Functionalization of Graphene Nanoribbon Stacks

Bostjan Genorio,[†,⊥] Wei Lu,[†] Ayrat M. Dimiev,[†] Yu Zhu,[†] Abdul-Rahman O. Raji,[†] Barbara Novosel,[⊥] Lawrence B. Alemany,[†,∥,§] and James M. Tour[†,‡,§,*]

[†]Department of Chemistry, [‡]Department of Mechanical Engineering and Materials Science, [∥]Shared Equipment Authority, and [§]Richard E. Smalley Institute for Nanoscale Science and Technology, Rice University, 6100 Main Street, Houston, Texas 77005, United States, and [⊥]Faculty of Chemistry and Chemical Technology, University of Ljubljana, Aškerčeva cesta 5, 1000 Ljubljana, Slovenia

ABSTRACT

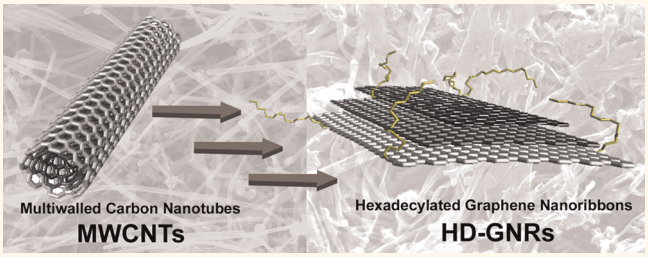

A cost-effective and potentially industrially scalable, *in situ* functionalization procedure for preparation of soluble graphene nanoribbon (GNRs) from commercially available carbon nanotubes is presented. The physical characteristics of the functionalized product were determined using SEM, evolved gas analysis, X-ray diffraction, solid-state ^{13}C NMR, Raman spectroscopy, and GC–MS analytical techniques. A relatively high preservation of electrical properties in the bulk material was observed. Moreover, replacement of intercalated potassium with haloalkanes was obtained. While carbon nanotubes can be covalently functionalized, the conversion of the sp^2-hybridized carbon atoms to sp^3-hybridized atoms dramatically lowers their conductivity, but edge functionalized GNRs permit their heavy functionalization while leaving the basal planes intact.

KEYWORDS: graphene nanoribbon stacks · intercalation · alkylation · conductivity · edge functionalization

Graphene is a stable 2D material that holds great promise due to its having extraordinary electrical, mechanical, and thermal properties. Thus it is a potential building block for electronic devices. The abundance of carbon and its low toxicity are additional driving forces for the scientific community to search for applications of graphene in energy-related devices such as ultracapacitors, Li-ion batteries and solar cells and for catalysis.[1] However, two important issues need to be solved to realize the use of graphene and its derivatives in those future applications: (a) bulk preparation of high quality graphene-based nanomaterials and (b) functionalization and incorporation of these materials into devices.

Since the report in 2004,[2] many different methods have been developed to yield graphene nanomaterials. These methods can be divided into bottom-up and top-down strategies.[1] Bottom-up strategies include chemical vapor deposition (CVD) growth[3,4] and organic synthesis.[5] Both methods can deliver high quality and relatively low-defect materials but they are hard to scale-up and process. On the other hand there is the scalable top-down approach where graphite or carbon nanotubes (CNTs) are used as a starting material. The most common preparation method of bulk-quantity graphene is by exfoliation of oxidized graphite[6,7] with subsequent reduction[8] or high temperature annealing to produce more highly conjugated material.[9] The disadvantage of this method is the irreversible damage to the graphene basal plane and its consequently lower conductivity. High quality monolayer to few-layer graphene has been obtained in bulk quantities using different intercalation and thermal expansion techniques.[10–12] When tuning the physical properties and minimizing defects, one must also consider the shape of the material that is inherently governed by the graphite precursor for top-down approaches. It was reported that the width and edges of the graphene play important roles in defining the material's electronic properties.[13] CNTs are known precursors for production of bulk quantities of well-defined graphene nanoribbons (GNRs). To date several unzipping methods with reasonable yields have been reported.[14–18] Because of their high carbon aspect ratio, which is advantageous for mechanical processing, GNRs are good candidates for applications in

* Address correspondence to tour@rice.edu.

Received for review February 20, 2012 and accepted April 2, 2012.

Published online April 02, 2012
10.1021/nn300757t

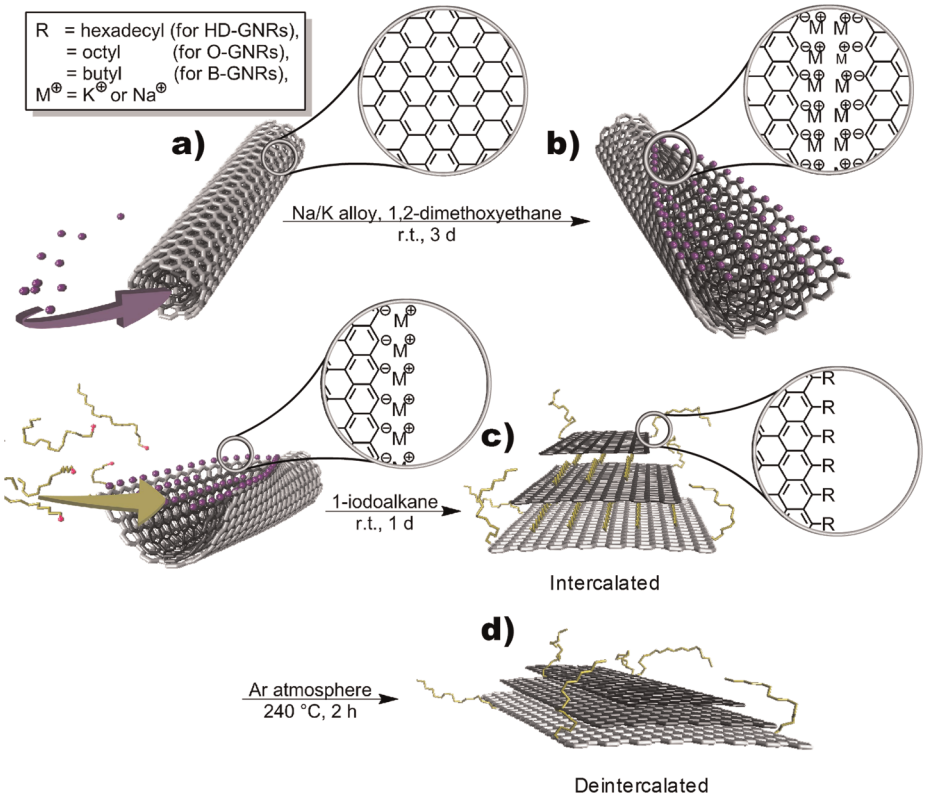

Figure 1. Proposed scheme for the *in situ* intercalation replacement and selective functionalization of GNRs: (a) intercalation of potassium between the walls of MWCNTs; (b) splitting process of MWCNTs and formation of active carboanionic edges (M = K^+ or Na^+); (c) *in situ* functionalization and intercalation of GNRs with alkyl groups; (d) deintercalation of functionalized GNRs.

energy related devices,[1] catalysis, transparent touch screens,[19] carbon fiber spinning,[20] formation of conductive polymer composites,[21] and low-loss-high-permittivity composites.[22] When dealing with applications, the material should be available in bulk quantities and should be easily processable, since most of the applications require preparation of well-dispersed solutions or suspensions. Pristine graphene materials are very difficult to disperse, thus functionalization is generally required.

Layered carbon materials such as graphite or multiwalled carbon nanotubes (MWCNTs) are stable because of their fully π-conjugated aromatic system. Traditional organic synthetic approaches are thus limited to certain reactions. Polycyclic aromatic hydrocarbons (PAHs), close chemical relatives to graphene-based materials, are susceptible to electrophilic substitutions, nucleophilic and free radical reactions, addition reactions, reductions, oxidations, and rearrangements.[23] All of these reactions could be used for functionalization of graphene. However, the current graphene literature reports are limited mostly to oxidation, hydrogenation, and reductive functionalization methods. These methods generally produce a product with the desired physical properties such as solubility and dispersibility. The degree of functionalization in these cases is relatively high, mostly because the basal planes are functionalized, but functionalization of the basal plane inevitably leads to a suppressed conductivity as the π-conjugation is disturbed. Selective edge functionalization might be a solution to this problem. However, edge functionalization would likely only have an impact on physical properties in materials with high edge-to-basal plane carbon ratios such as in GNRs.

In the present study we further investigate the hypothesis that potassium intercalation between the walls of commercial MWCNTs would longitudinally split the walls and furnish active carboanionic edges of the ribbons.[18] The increased reactivity of the edges compared to the basal plane would therefore preferably functionalize the edges of GNRs with desired electrophiles. Selective functionalization would introduce improved solubility without sacrificing conductivity. Further we investigate the replacement of intercalated metal with haloalkanes that then serve as intercalents in the resulting functionalized GNRs.

RESULTS AND DISCUSSION

The reaction scheme for the selective edge *in situ* functionalization is depicted in Figure 1. In the first step commercially available MWCNTs (Nanotech Laboratories, Inc. (NTL) or Mitsui & Co.) were treated with Na/K alloy in 1,2-dimethoxyethane (DME) for several days. Since K (but not Na) can be easily intercalated into graphene galleries[24] and Englert *et al.* have shown that

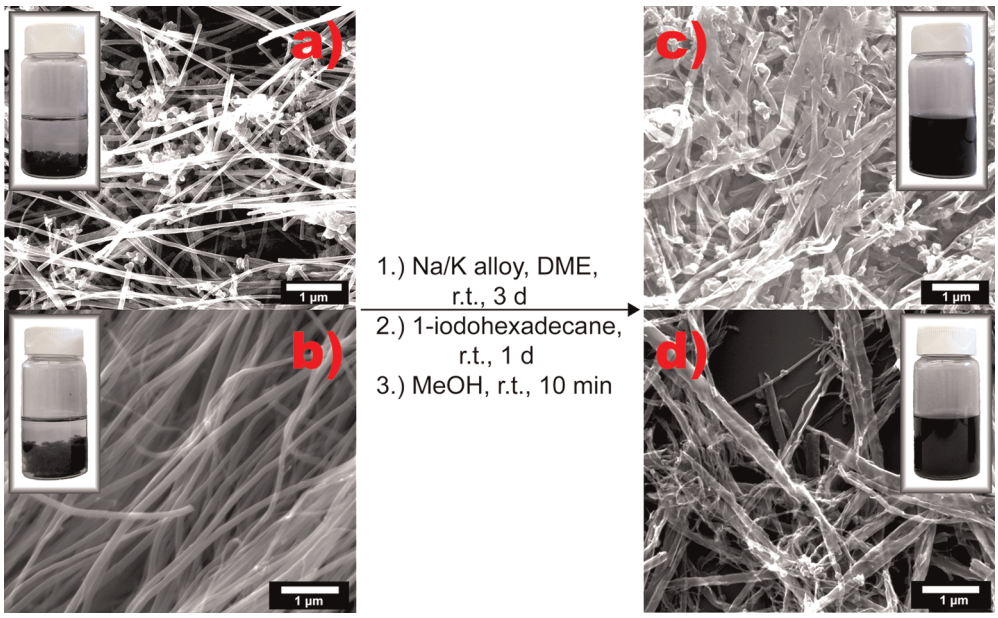

Figure 2. Solubility test. SEM images showing the splitting and functionalizing of commercially available MWCNTs and the photographic difference in solubility between functionalized GNRs and pristine MWCNTs: (a) pristine Mitsui MWNTs and a 0.1 mg/mL suspension in chloroform; (b) pristine NTL MWNTs and a 0.1 mg/mL suspension in chloroform; (c) Mitsui-originated HD-GNRs and a 0.1 mg/mL stable dispersion in chloroform; (d) NTL-originated HD-GNRs and a 0.1 mg/mL stable dispersion in chloroform.

K can be successfully intercalated into graphite flakes using the above conditions,[25] we also expected K to intercalate between the walls of the MWCNTs. Our previous work has shown that the intercalation of the K is accompanied by partial longitudinal cracking of the walls as they tend to swell.[18] Under the conditions used, the edge atoms should be in the reduced carboanionic form and thus very reactive and susceptible to electrophilic attack. This reductive splitting can be visualized as the reaction mixture changes color from a dark black or brown color to a finely dispersed green or red suspension. The next step is the *in situ* functionalization; iodoalkanes (1-iodohexadecane, 1-iodooctane, and 1-iodobutane) are added to the reaction mixtures, presumably reacting with the active sites on the edges of the GNRs. As the reaction proceeds, the green or red color disappears. To produce proton functionalized GNRs (H-GNRs) we quenched the reaction mixture with methanol (described in detail in the Supporting Information). To attain the intercalated compounds with a formula as close as possible to KC_8 or stage 1,[18] an excess of Na/K was used. Accordingly, it was necessary to add an excess of the iodoalkanes. This leads to side reactions, not just in the reaction solution, but also between the walls of the MWCNTs. The side products include alkanes, alkenes, and dimers of alkanes. SEM images clearly indicate that MWCNTs split to GNRs (Figure 2) in high yields. To quench any active species that were remaining, we treated the reaction mixture with methanol. The crude materials, hexadecylated-GNRs (HD-GNRs), octylated-GNRs (O-GNRs), and butylated-GNRs (B-GNRs), were collected by filtration using 0.45 μm PTFE-membranes and the filter cakes were washed with organic solvents and water and then underwent Soxhlet extraction to remove the majority of the physisorbed impurities. Before analysis, all of the products were dried in vacuum ($\sim 10^{-2}$ Torr) at 60 °C for 24 h. To the best of our knowledge, a similarly efficient *in situ* one-pot method of converting MWCNTs to functionalized GNR stacks has not been reported. The efficiency of the synthesis and possible scale-up makes it further attractive.

Bulk Properties. The solubility of pristine graphitic materials is in general known to be poor. For bulk purposes, dispersing of the material is of great importance. For our solubility study, we focused on HD-GNRs. HD-GNRs exhibit an improvement in solubility and dispersibility in chloroform after a short sonication using simple ultrasonic cleaner. In Figure 2, where starting MWCNTs were compared to HD-GNRs, the difference is apparent. HD-GNRs show stable dispersions in chloroform for weeks, while MWCNTs cannot be dispersed using the same conditions. We have also performed solubility test for HD-GNRs and MWCNTs at 0.1 mg/mL concentrations in different solvents (Supporting Information Figure S1). HD-GNRs are well dispersible in common organic solvents such as 2-propanol, acetone, ethyl acetate, diethyl ether, chloroform, hexane, and chlorobenzene. After 1 h, HD-GNRs settle out in hexanes and diethyl ether, while remaining dispersed in the other solvents. Four days of shelf aging resulted in sedimentation of all of the suspensions except when in chloroform and chlorobenzene,

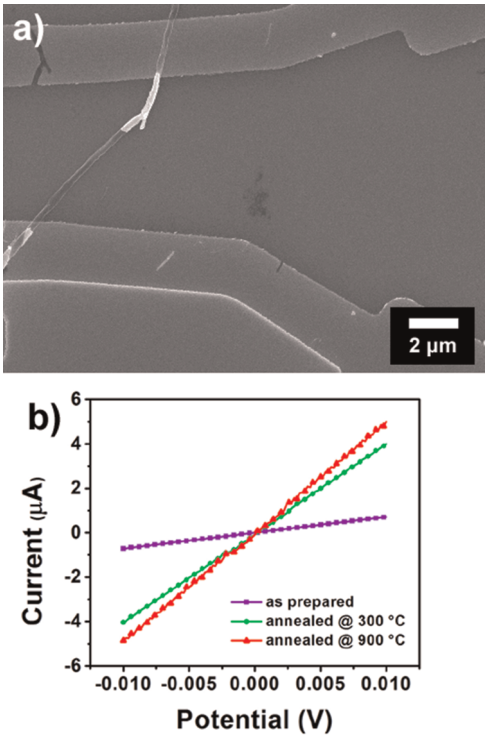

Figure 3. Fabricated device and conductivity measurements: (a) SEM image of a device made from HD-GNRs stack; NTL-originated MWCNTs and Pt electrodes; (b) change in electrical properties after different thermal treatment compared to as-prepared HD-GNRs.

which stayed well-dispersed for weeks. A low magnification SEM image and optical microscope image of drop cast HD-GNRs on a SiO_2/Si substrate show well-dispersed material (Supporting Information Figure S2). However, the starting material MWCNTs showed sedimentation in all solvents tested in less than 1 h. Thus HD-GNRs are good candidates for applications where organic dispersibility is important.

Conductivity. A desirable property in functionalized GNRs is the retention of conductivity especially if they are to be used in transparent electrodes or energy-related devices such as ultracapacitors, Li-ion batteries, and solar cells. We have fabricated a single HD-GNR device by depositing 20 nm thick Pt contacts on opposite ends of GNR stacks using lithography (Figure 3a). The HD-GNR stack used in the device was 7.9 μm long, ~300 nm wide (Supporting Information Figure S3), and ~30 nm thick. The thickness was estimated from the AFM image (Supporting Information Figure S4). The as-prepared, single ribbon device exhibited a conductivity of 600 S/cm (Supporting Information eq S1 and Table S1). The conductivity increased almost six times to 3540 S/cm when the device was annealed at 300 °C. There are at least two reasons for such a difference in conductivity between the as-prepared sample and the sample annealed at 300 °C. The conductivity could be partially increased due to improved contact between the electrodes and the GNR stack. However, previous work on graphene materials with Pt-contacts shows that the good wetting of the carbon with Pt leads to a low-barrier contact,[18] thus the main contribution is probably due to deintercalation of hydrocarbons (but not necessarily defunctionalization) from the graphene galleries. The intercalated graphene galleries are electrically isolated from each other, as alkanes are known insulators; deintercalation reinstates the interaction between the graphene layers. A control experiment where HD-GNRs were heated at 300 °C for 2 h showed that their solubility in chloroform after annealing was comparable to the as-prepared HD-GNRs. The latter result speaks in favor of the HD functional groups staying intact at temperatures up to 300 °C. When the device was further heated to 900 °C, a temperature at which the HD functional groups are expected to have cleaved from the GNRs, the conductivity increased to 4260 S/cm. This small increase could indicate that edge functionalization does not substantially disturb the conductivity of the graphene basal planes. The conductivities of the functionalized HD-GNRs are comparable to previous literature reports on pristine materials such as graphite (200−8300 S/cm),[26] CNTs (1000−100000 S/cm),[27] and GNRs (~800 S/cm)[13,18,28] and thus interesting for further study. Bulk conductivities of as-prepared samples were also measured using four-point probe measurement on pressed pellet. Similarly, relatively high conductivity ranging from 145 to 175 S/cm was observed, which is only 2.5 times smaller than conductivities of the starting material MWCNTs (Supporting Information Figure S5, Scheme S1 and eq S2).

Evolved Gas Analysis (EGA). Confirming edge functionalization *versus* intercalation remains challenging due to the expected low degree of edge carbons to non-edge carbons. The average GNRs stack with 250 nm width × 2.7 μm length dimensions (estimated from the SEM image, Supporting Information Figure S3) should have only 0.05 atomic % of edge carbons in GNRs (Supporting Information Figure S6). If all of the edge carbons are functionalized then the functional groups would contribute 1 wt % of the total weight to the HD-GNRs; 0.5 wt % if considering O-GNRs, and 0.25 wt % if considering B-GNRs. Since the expected degree of functionalization is low, we have used thermogravimetric analysis (TGA) coupled with a quadrupole mass spectrometer (QMS) to detect thermalized products. The sensitivity of QMS should give some insight into the quantitative nature of the alkylated graphene nanoribbons (A-GNRs). The TGA of HD-GNRs shows a total weight loss of 37% in the range between 40 and 900 °C, which is far above the expected value of 1% (Figure 4a). The reference compound, hexadecane, has a specific fragmentation pattern, with high abundance fragments with decreasing intensities at m/z = 57, 43, 71, 85, 29, and 99. Similar patterns are expected for octane m/z 43, 57, 29, 85, 71 and for butane m/z 43, 29, 15, 57.

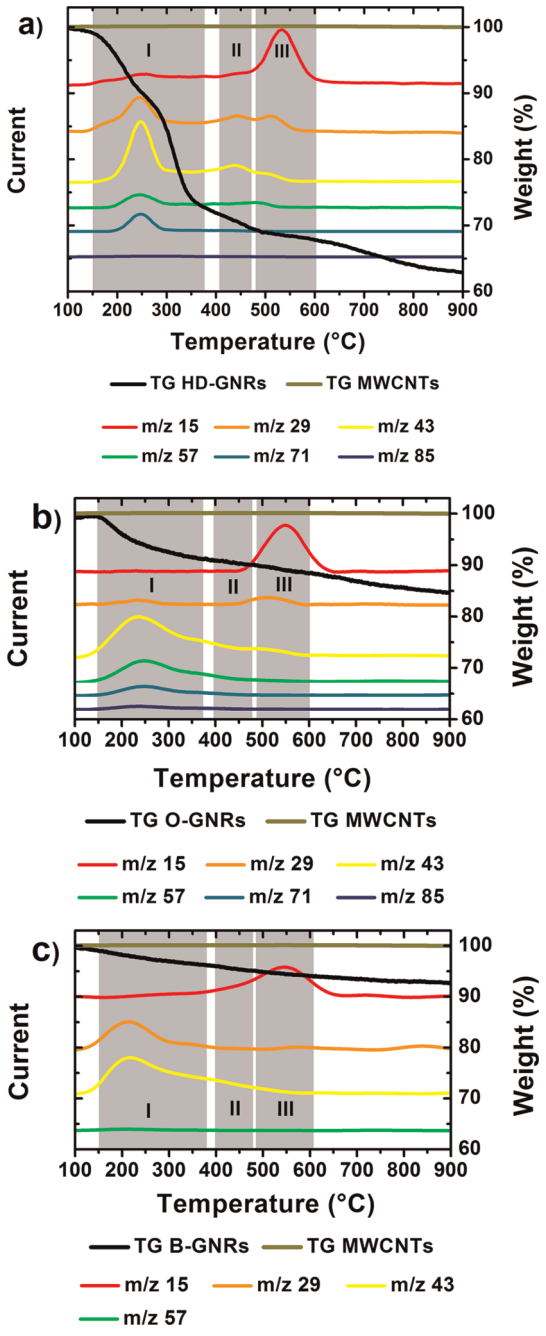

Figure 4. Evolved gas analysis. Different colors represent fragments with *m/z* that correspond to alkane fragments. Black and gold curves represent the TGA profile of functionalized GNRs and pristine MWCNTs, respectively. Gray rectangles represent region I, region II, and region III, respectively. (a) TGA-MS of HD-GNRs; (b) TGA-MS of O-GNRs, and (c) TGA-MS of B-GNRs.

These fragments were also found in the evolved gases during the TGA, indicating that alkyl groups are present in the A-GNRs samples (Figure 4). However, there are three distinct temperature ranges during which the alkyl groups are present in the off-gas from HD-GNR thermolysis products (Figure 4a). The first is the range between 154 and 374 °C (region I), where the weight loss is 26%. The second range is between 400 and 474 °C with a weight loss of 2% (region II) while the range between 480 and 612 °C had a 2% weight loss (region III). Region I is assigned to deintercalation of alkanes; see what follows for further explanation. Regions II and III were assigned to covalently bound alkyl groups, most likely hexadecyl. The temperature interval for region II corresponds with previous reports on covalently attached organic moieties on different carbon substrates.[25,29] The mass spectrometer detection limit is up to 100 atomic mass units; thus the molecular ion corresponding to the hexadecyl moiety could not be detected. Fragments *m/z* 29, 15, 43, 57, 85, and 71 that are present in region II are indications that fragmentation due to thermal cleavage of the hexadecyl group is most likely occurring. The major fragments present in region III are the methyl and ethyl groups (*m/z* 15, 29) which could be the remainder of the hexadecyl group bound directly to the graphene substrate. Similar results were obtained for O-GNRs and B-GNRs (Figure 4b,c), where we observed 7 wt % loss between 139 and 293 °C, and 4 wt % between 121 and 247 °C for region I, respectively. Region II between 448 and 526 °C for O-GNRs shows a 1 wt % loss, while region III between 526 and 628 °C had a 1.3 wt % loss. B-GNRs show 1.3 wt % loss for region II between 328 and 453 °C and 1.7 wt % for region III between 453 and 636 °C. According to this data and the assumption that regions II and III correspond to the same functional groups but have different fragmentation temperatures, the degree of functionalization is 4.6% for HD-GNRs, 2.3% for O-GNRs, and 3% for B-GNRs. The reason for the discrepancy between the estimated degree of edge functionalization and the actual degree of functionalization is unclear.

To exclude the reaction between solvent and active GNRs, the EGA of methanol-quenched, thus hydrogen terminated, GNRs (H-GNRs) was also done. TGA-MS analysis confirmed the absence of all fragments except *m/z* 15, the methyl fragment between 400 and 600 °C (Supporting Information Figure S7). The methyl fragment could be the result of rearrangements with successive cleavage on defects and edges where carbons are expected to be hydrogen-terminated or from trace methanol.[14]

X-ray Powder Diffraction (XRD) Analysis. For direct evidence of deintercalation in region I, HD-GNRs thermally treated at temperatures of 240, 530, and 900 °C were prepared, and XRD diffractograms were recorded and analyzed (Figure 5a). The total weight loss for the sample heated at 240 °C for 2 h was 26%, which corresponds to the weight loss in region I in Figure 4a. For the sample heated at 530 °C for 2 h, the weight loss was 32%, and for the sample heated at 900 °C for 20 min, the weight loss was 39% (for the TGA plots of the thermally treated HD-GNRs samples see Supporting Information Figure S8).

The XRD diffractogram for the as-prepared sample contains well-pronounced diffraction lines at 12.0° and

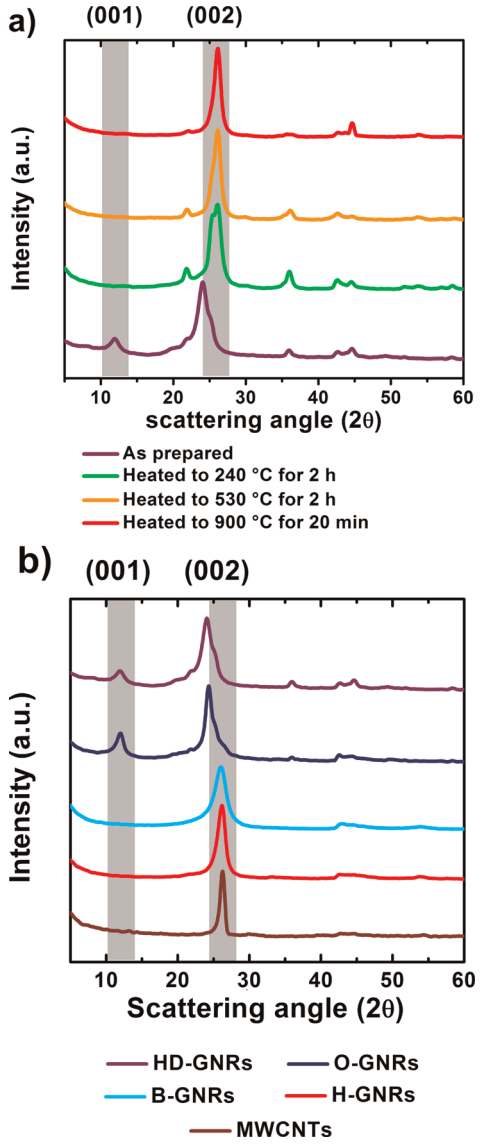

Figure 5. Powder diffraction patterns. (a) Comparison of as-prepared intercalated HD-GNRs and thermally treated HD-GNRs where deintercalation is observed. (b) Comparison of functionalized HD-GNRs, O-GNRs, B-GNRs, GNRs, and MWCNTs. Peaks at 21.8°, 25.3°, 35.9°, 42.4°, 44.4°, 51.8°, 56.8°, and 58.4° 2θ angle correspond to low concentrations of KI impurity, which could not be removed.

24.2° 2θ angle, which correspond to the (001) and (002) signals of a stage 1 intercalation compound, respectively. The calculated *c*-axis repeat distance (I_c) is 0.738 nm, which is the typical spacing (d_s) between the two carbon layers sandwiching the layer of intercalant. As one can see from Figure 5a, both the 12.0° and 24.2° signals disappear after heating at 240 °C. The new diffraction line at 26.2° 2θ angle corresponding to the (002) signal of graphite appears instead.

The sample heated to 240 °C and then cooled to room temperature can be considered an intermediate state between the fully intercalated as-prepared sample and the one heated for 2 h at 240 °C. The weight loss during heating to 240 °C was ~12% (Supporting Information Figure S8). The sample that was heated and then cooled contains both the 24.2° signal and the 26.2° signal in a ratio of ~1:2 (Supporting Information Figure S12). Interestingly, no intermediate stage compound was detected in the sample. This is very unusual for graphite intercalation compounds (GICs), where graphite gradually intercalates and then gradually deintercalates, sequentially going through all the stage numbers.[24] Instead we detect only the two states, the stage 1 GIC and the nonintercalated graphitic GNRs. We suggest that the mixed stage comes from different GNRs. Individual GNRs probably deintercalate quickly and completely; the observed "mixed stage" is simply a mixture of completely intercalated and completely deintercalated individual GNR stacks. Samples heated at temperatures of 530 and 900 °C are completely deintercalated and give diffractograms identical to H-GNRs or the starting material MWNTs (Figure 5b). Since weight losses of 7% and 4% were also observed for O-GNRs and B-GNRs in region I, XRD diffractograms were also recorded for as-prepared samples. However, O-GNRs show similar intercalation compounds as HD-GNRs, with I_c spacing between graphene layers of 0.731 nm. Interestingly, B-GNRs do not show any intercalation (Figure 5b), since the diffractograms are identical to H-GNRs or MWNTs. The reason might be in the size of the intercalant. In the case of HD-GNRs, it is expected to be at least 16 or 32 carbon chains (the latter is the dimer product). Hexadecane and octane are higher boiling point liquids while dotriacontane is a solid. On the other hand butane is a gas which is likely too volatile and mobile to form a stable GIC. For HD-GNRs, the proposed major intercalant is dotriacontane, but others cannot be excluded. The synthesis of HD-GNRs, as discussed earlier, leads to side products that are also potential intercalents. Two control experiments produced evidence that dotriacontane is indeed the main component. In the first control experiment 1-iodohexadecane was added into the dispersion of Na/K in DME (Supporting Information). Gas chromatography–mass spectrometry (GC–MS) showed the presence of 1-hexadecene and hexadecane as minor components (21% and 19%, respectively) and dotriacontane as the major component (60%) of the reaction mixture. Another experiment with as-prepared HD-GNRs was done. HD-GNRs were heated at 150 °C in vacuum. A coldfinger cooled to 0 °C was connected to the system to capture products that were released. Analysis of the collected vapors using GC–MS again showed dotriacontane as the major component (45%). Other components detected were 1-hexadecene (6%), hexadecane (35%), and starting material 1-iodohexadecane (13%, for the GC–MS analysis see Supporting Information Figure S9).

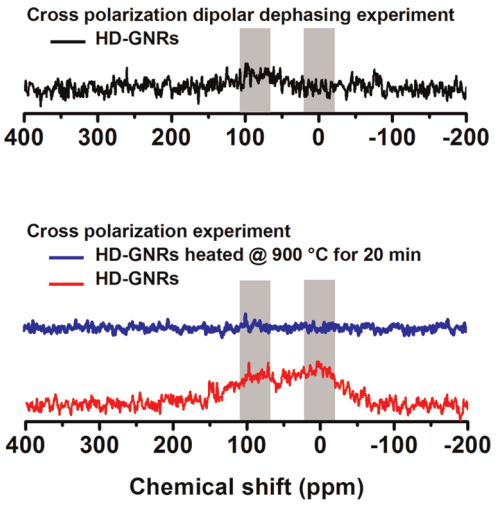

Figure 6. SS NMR. Cross-polarization experiment of functionalized and intercalated HD-GNRs (red curve) and defunctionalized and deintercalated HD-GNRs after heating at 900 °C for 20 min (blue curve). Cross-polarization dipolar dephasing experiment of functionalized and intercalated HD-GNRs (black curve).

Solid-State ^{13}C Nuclear Magnetic Resonance Spectroscopy (SS NMR). To further investigate the nature of the intercalent, two types of magic angle spinning (MAS) NMR experiments were performed. The relatively high conductivity of HD-GNRs caused severe probe tuning problems, which initially prevented useful $^{1}H-^{13}C$ cross-polarization (CP) and direct ^{13}C pulse spectra from being obtained. However, dispersing the sample in silica (an approach previously used to obtain a ^{13}C spectrum of graphite[30]) enabled the ^{13}C and ^{1}H channels to be properly tuned on a sample of 10 wt % HD-GNRs and 90 wt % silica.

In the CP spectrum of the unheated material (Figure 6, red spectrum), two broad, overlapping bands are evident. The band centered at about 90 ppm is thought to be from several types of carbons: graphene sheet sp^2 C−H carbons, graphene sheet sp^2 carbons that are either on or near the edge of the sheet or near a covalently bound hexadecyl group or intercalated alkane and thus are capable of being cross polarized, and from the downfield tail of the signal from the methylene carbons in covalently bound hexadecyl groups and in intercalated side products (*e.g.*, hexadecane, 1-hexadecene, and dotriacontane). The band centered at about 90 ppm is unusually broad and shielded, as is the signal from the carbons detected in a direct ^{13}C pulse spectrum of graphite dispersed in silica.[30] The breadth of the band centered at about 90 ppm can be at least partially attributed to the inability of MAS to completely remove the anisotropy of the magnetic susceptibility in the graphene sheets,[30,31] while the shielding can be attributed to the diamagnetic shift in the δ_{33} component of the shielding tensor of the numerous graphene carbons in a very large condensed aromatic ring system.[31] This broadening and shielding is reminiscent of what is observed as graphite oxide is steadily reduced and becomes increasingly like graphite.[32]

The band centered at about 0 ppm is thought to be from the methylene carbons indicated above and from the upfield tail of the signal from graphene sheet sp^2 carbons. The band centered at about 0 ppm is also unusually shielded, as would be expected if the covalently bound hexadecyl groups or intercalated alkanes are sandwiched between the graphene sheets and thus are subjected to a large diamagnetic susceptibility resulting from delocalized electrons (a π-electron ring current) in the graphene sheets. Indeed, a less dramatic shielding effect but much better resolution is observed with anthracite bearing dodecyl groups on the edges.[33] In contrast, the central methylene carbons in the methylene chains constrained to be above an aromatic ring in molecules such as [12]-paracyclophane[34] and various 1,*n*-dioxa[*n*](2,7)pyreneophanes[35] experience only a very small ring current shielding effect. The much weaker signal from the methyl carbons in the HD-GNRs is not recognizable.

The 50-μs dephasing period in the dipolar dephasing experiment on the unheated material (Figure 6, black spectrum) strongly attenuates the band centered at about 90 ppm and completely eliminates the band centered at about 0 ppm. Since this dephasing period is designed to eliminate CH and CH_2 signals with minimal attenuation of quaternary carbon signals,[33] the less shielded band in the basic (red) CP spectrum has significant contributions from graphene sheet sp^2 C−H carbons and the downfield tail of the signal from the various methylene carbons, while the more shielded band in the basic CP spectrum is consistent with the various methylene carbons and the upfield tail of the signal from graphene sheet sp^2 C−H carbons. The relatively immobile nature of the covalently bound hexadecyl groups and intercalated alkanes results in a correspondingly strong $^{1}H-^{13}C$ dipole−dipole interaction that both makes it possible for these methylene groups to cross polarize (red spectrum) and then to have the signal rapidly decay (black spectrum). The very weak signal centered at about 90 ppm in the dephasing experiment may result from the attenuated signal from graphene sheet sp^2 carbons that poorly cross polarized.

The CP spectrum of the heated material (Figure 6, blue spectrum) shows no signal above the noise. As seen from the conductivity, TGA, and XRD results, defunctionalization and deintercalation at this temperature is complete. With no covalently bound hexadecyl groups or intercalated alkanes remaining, no NMR signal is detected. The importance of these hexadecyl groups and alkanes for generating the signals in the spectrum of the unheated material (red spectrum) is evident.

Raman Spectroscopy. The Raman spectrum of the as-prepared sample is significantly enhanced compared

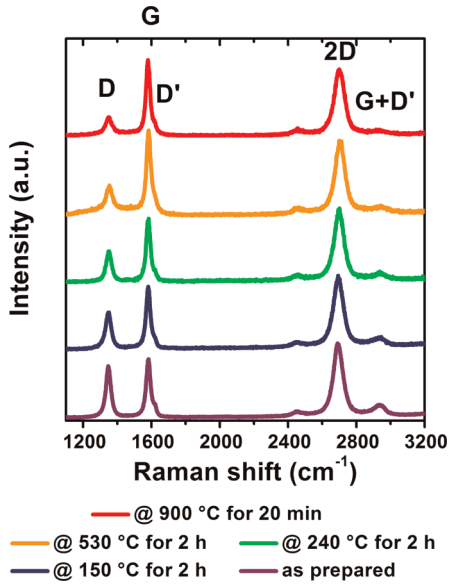

Figure 7. Raman spectra. Comparison of thermally treated HD-GNRs with as-prepared sample.

to the heated samples (Figure 7). This is an additional argument in support of formation of the intercalation compound. It is known that when several species are intercalated into graphite, or simply physisorbed on the graphene surface, the Raman spectra are enhanced.[36,37] No blue-shift of the G-peak is detected, however. This suggests that the intercalant in HD-GNRs is neutral toward carbon and does not charge the carbon layers. The spectrum of the as-prepared sample contains a D-peak at ~1360 cm^{-1} of very high intensity and the G+D′ peak at ~2950 cm^{-1}. This suggests that significant disorder in the system was induced by splitting[17] and intercalation. This is rather unusual, because for most of the known GIC compounds, intercalation does not cause appearance of the D-band. The D-band gradually decreases with heating and is finally of the same magnitude as nonintercalated split GNRs. The D/G ratio can be considered a measure of disorder. The fact that it decreases suggests that disorder induced by the intercalant decreases when the intercalant is removed. The 2D peak in both the parent MWCNTs and GNRs is single-Lorentzian, suggesting no AB stacking. This is quite natural, since the walls in MWCNT have different chiralities. They retain their structure after splitting. Hence, the layers in the GNR have some degree of single-layer character.

We hypothesize that intercalation is possible only when the reaction of intercalated K and 1-iodoalkane occurs between graphene sheets. The byproduct KI is forced out, while newly formed alkanes and alkenes (as well as covalently bound alkyl groups) take their places between sheets. For this process the term "replacement-driven intercalation" is introduced. To partially confirm the latter, we performed a control experiment, where instead of 1-iodohexadecane, hexadecane was used (Supporting Information page S14). Under the same reaction conditions, no intercalation was observed, and that was confirmed by XRD (Supporting Information Figure S10), where the (002) signal was observed at 26.2° 2θ angle, which corresponds to nonintercalated material, and by TGA, where we observed a weight loss of ~2% in the region between room temperature and 800 °C (Supporting Information Figure S11).

CONCLUSIONS

A high yielding conversion of commercially available MWCNTs to *in situ* functionalized GNR stacks was achieved by a reductive method. GNRs bearing long alkyl chains are well-dispersible in organic solvents such as alcohols, ketones, ethers, and alkanes. Particularly stable dispersions are produced in chloroform or chlorobenzene. HD-GNRs exhibit relatively high GNR conductivity as well as bulk material conductivity. The conductivity of ~3540 S/cm of single deintercalated HD-GNR was achieved through minimal interruption of the conjugated π-system of the basal plane. Therefore we propose that functionalization occurs preferably on the edges of graphene. The concept of edge functionalization was partially supported by EGA, enhanced solubility, and relatively high conductivity of single and bulk-functionalized material. Replacement of intercalated addends was observed and thoroughly investigated for the HD-GNRs and O-GNRs. TGA-MS showed deintercalation of alkanes and alkenes at temperatures between 140 and 300 °C. XRD revealed a stage 1 intercalation compound for the as-prepared samples. Interestingly, no intermediate stage compounds were detected. GC−MS showed dotriacontane as a major intercalant compound in HD-GNRs. Further, solid-state ^{13}C nuclear magnetic resonance spectra of HD-GNRs were consistent with the presence of methylene carbons in covalently bound hexadecyl groups and intercalated alkanes, as the signal attributed to the methylene carbons is unusually shielded and disappears after the sample is deintercalated and defunctionalized by heating. Similarly, Raman spectroscopy for the as-prepared sample indicated the intercalation compound. XRD and Raman spectroscopy revealed that thermal treatment of intercalated HD-GNRs up to ~300 °C leads to full deintercalation. However, covalently bound functional groups are stable at that temperature and still provide enhanced solubility, as the deintercalated HD-GNRs are still soluble in organic solvents. Functionalized GNRs with enhanced properties such as dispersibility and conductivity should be of great interest for bulk application as well as further basic research since improved processability and scale-up is possible. Possible fields of application are catalysis, ultracapacitors, transparent touch screens, carbon fiber spinning, formation of conductive polymer

composites, and low-loss, high-permittivity composites. Further, the intercalation and functionalization principle could be used in the field of organic-based Li-ion batteries where the intercalant or addend would bear the redox center, as the method enables variations in functional addends.

EXPERIMENTAL SECTION

Materials. Reactions were performed in dried glassware under an N_2 atmosphere unless stated otherwise. Reagent grade 1,2-dimethoxyethane was degassed with Ar, refluxed over sodium in an N_2 atmosphere, and freshly distilled. Other solvents were used without further distillation. Mitsui MWCNTs were received from Mitsui & Co. (lot no. 05072001K28). NTL-M grade MWCNTs were donated by Nanotech Laboratories, Inc. (5T10M10). All other commercially available reagents were used as received. Liquid Na/K alloy was prepared in a vial inside of a N_2 glovebox by pressing together freshly cut K (1 mol equiv) and Na (0.22 mol equiv) chunks using tweezers to facilitate the melting process. Amounts of liquid Na/K alloy indicated are by volume. *Caution: All synthetic steps involving Na/K alloy should be carried out with extreme caution under strict exclusion of air or moisture and under inert gas and appropriate personal protection (hood, blast shields, face shield, protective and fire resistant clothing) should be used and worn at all times.* 1-Iodohexadecane, 1-iodooctane, and 1-iodobutane were all obtained from Sigma-Aldrich and used as received without further purification. In-house deionized water was used during purification of the products.

Synthesis of Functionalized Graphene Nanoribbons Stacks and Intercalation Replacement. A sample of MWCNTS (100 mg, 8.3 mmol) was added to an oven-dried 250 mL round-bottom flask containing a magnetic stir bar. The vessel was then transferred to a N_2 glovebox where freshly distilled 1,2-dimethoxyethane (35 mL) and liquid Na/K alloy (0.29 mL) were added. The flask containing the suspension was then sealed with a septum and transferred out of the glovebox where the suspension was dispersed by a short 5 min ultrasonication (using ultrasonic cleaner Cole-Parmer model 08849-00) to yield a dark greenish to red suspension. After ultrasonication, the reaction mixture was vigorously stirred (450 rpm) at room temperature for 3 d. The reaction suspension was then quenched by the addition of the 1-iodoalkane (8.75 mmol) through a syringe and left to stir at room temperature for an additional day. Methanol (20 mL, 500 mmol) was then added to quench any excess Na/K alloy, and the mixture was stirred at room temperature for 10 min. For workup, the reaction mixture was filtered over a 0.45 μm pore size PTFE membrane. The filter cake was successively washed with THF (100 mL), *i*-PrOH (100 mL), H_2O (100 mL), *i*-PrOH (100 mL), THF (100 mL) and Et_2O (10 mL). Then Soxhlet extraction with THF was used for 3 d, and the product was dried in vacuum ($\sim 10^{-2}$ mbar) for 24 h.

Electron Microscopy. Samples were dispersed in chlorobenzene and bath sonicated using an ultrasonic cleaner for 15 min for a quick dispersion. A drop was cast on a 100 nm SiO_2/Si substrate, and large area low resolution images were taken at 20 kV under FEI Quanta 400 ESEM FEG scanning electron microscope and under a JEOL-6500 field-emission microscope.

Conductivity Measurements. Fabrication of HD-GNR devices was performed by tracking individual GNRs on the surface of 500 nm-thick thermal SiO_2 layer-covered highly doped Si substrates by SEM (JEOL-6500 microscope), followed by the patterning of 20 nm-thick Pt contacts by standard electron beam lithography. The electrical transport properties were tested using a probe station (Desert Cryogenics TT-probe 6 system) under vacuum with a chamber base pressure below 10^{-5} Torr. The *I*–*V* data were collected by an Agilent 4155C semiconductor parameter analyzer.

Evolved Gas Analysis (EGA) Experimental Part. Thermogravimetric measurements were performed on a Netzsch 449 F3 Jupiter instrument under a dynamic Ar (5.0) flow with a flow rate of 60 mL/min in a temperature range from 25 to 900 °C. A heating rate of 10 K/min was used. About 5 mg of sample was placed in an alumina (Al_2O_3) crucible. Simultaneously mass spectrometry was performed on MS 403C Aëolos with a SEM Chenneltron detector and system pressure of 2×10^{-5} mbar. Gasses that evolved under TG heat treatment were transferred to the mass spectrometer through transfer capillary, quartz ID 75 μm, which was heated up to 220 °C. The upper limit of the mass spectrometer detector was 100 AMU.

XRD. X-ray powder diffraction (XRD) was performed using a Rigaku D/Max 2550 diffractometer with Cu Kα radiation (λ = 1.5418 Å). Where necessary the data obtained were analyzed and processed using the Jade 9 software package.

GC–MS. GC–MS was performed on Agilent Technologies 6890N Network GC system coupled to an Agilent 5973 network mass selective detector.

SS ^{13}C NMR Spectroscopy. Spectra were obtained at 50.3 MHz ^{13}C on a Bruker Avance 200 spectrometer with a probe for magic angle spinning (MAS) of rotors 4 mm in diameter. Chemical shifts are relative to the carbonyl carbon in glycine defined as 176.46 ppm.[38] Both samples in Figure 6 were dispersed in silica (10 wt % sample, 90 wt % silica). Parameters for the ^{1}H–^{13}C CP spectrum of functionalized and intercalated HD-GNRs (red curve in Figure 6): 7.6 kHz MAS (so that any spinning sidebands are at multiples of +151 or −151 ppm from a centerband), 90° ^{1}H pulse = 2.4 μs, contact time = 1 ms with ramped amplitude proton pulse, FID = 32.8 ms with spinal64 decoupling, relaxation delay =5 s, number of scans =40 400, line broadening = 50 Hz (1 ppm) used in processing the FID. Parameters for the ^{1}H–^{13}C CP/dipolar dephasing spectrum of functionalized and intercalated HD-GNRs (black curve in Figure 6): as above except that a pair of 25-μs dephasing periods with a central 8.3-μs, 180° ^{13}C refocusing pulse immediately preceded FID acquisition. Parameters for the ^{1}H–^{13}C CP spectrum of functionalized and intercalated HD-GNRs heated at 900 °C for 20 min (blue curve in Figure 6) are the same as for the unheated sample (red curve) except for 85 000 scans. Parameters for the ^{1}H–^{13}C CP spectrum of 100% silica (control sample) are the same except for 55 000 scans; no signal was detected.

Raman Spectroscopy. The Raman spectra were acquired using a Renishow Raman RE01 microscope with 40× lens; 514 nm wavelength laser was used for excitation.

Conflict of Interest: The authors declare no competing financial interest.

Supporting Information Available: Additional synthesis details, optical, SEM, AFM images, conductivity measurements, TGA, GC–MS, and XRD of the described materials. This material is available free of charge *via* the Internet at http://pubs.acs.org.

Acknowledgment. We thank MI-SWACO, the Advanced Energy Consortium (BG Group, Halliburton, Conoco Phillips, bp, OXY, Marathon, Shell, Total, Petrobras, Schlumberger), the AFOSR (FA9550-09-1-0581), Center of Excellence Low Carbon Technologies, Slovenia (CO NOT), Center of Excellence Advanced Materials and Technologies for the Future, Slovenia (CO NAMASTE), the Lockheed Martin Corporation through the LANCER IV Program, NSF (CHE 0947054), and the ONR MURI program (Grant Nos. 00006766, N00014-09-1-1066) for funding. We thank Drs. A. Tanioka and M. Endo for the donation of the Mitsui MWCNTs, and Nanotech Laboratories, Inc. for the NTL MWCNTs.

REFERENCES AND NOTES

1. Luo, B.; Liu, S.; Zhi, L. Chemical Approaches toward Graphene-Based Nanomaterials and Their Applications in Energy-Related Areas. *Small* **2011**, 10.1002/smll.201101396.
2. Novoselov, K. S.; Geim, A. K.; Morozov, S. V.; Jiang, D.; Zhang, Y.; Dubonos, S. V.; Grigorieva, I. V.; Firsov, A. A.

Electric Field Effect in Atomically Thin Carbon Films. *Science* **2004**, *306*, 666–669.
3. Li, X.; Cai, W.; An, J.; Kim, S.; Nah, J.; Yang, D.; Piner, R.; Velamakanni, A.; Jung, I.; Tutuc, E.; *et al*. Large-Area Synthesis of High-Quality and Uniform Graphene Films on Copper Foils. *Science* **2009**, *324*, 1312–1314.
4. Yu, Q.; Jauregui, L. A.; Wu, W.; Colby, R.; Tian, J.; Su, Z.; Cao, H.; Liu, Z.; Pandey, D.; Wei, D.; *et al*. Control and Characterization of Individual Grains and Grain Boundaries in Graphene Grown by Chemical Vapour Deposition. *Nat. Mater.* **2011**, *10*, 443–449.
5. Wu, J.; Pisula, W.; Müllen, K. Graphenes as Potential Material for Electronics. *Chem. Rev.* **2007**, *107*, 718–747.
6. Hummers, W. S.; Offeman, R. E. Preparation of Graphitic Oxide. *J. Am. Chem. Soc.* **1958**, *80*, 1339–1339.
7. Marcano, D. C.; Kosynkin, D. V.; Berlin, J. M.; Sinitskii, A.; Sun, Z.; Slesarev, A.; Alemany, L. B.; Lu, W.; Tour, J. M. Improved Synthesis of Graphene Oxide. *ACS Nano* **2010**, *4*, 4806–4814.
8. Stankovich, S.; Dikin, D. A.; Piner, R. D.; Kohlhaas, K. A.; Kleinhammes, A.; Jia, Y.; Wu, Y.; Nguyen, S. T.; Ruoff, R. S. Synthesis of Graphene-Based Nanosheets *via* Chemical Reduction of Exfoliated Graphite Oxide. *Carbon* **2007**, *45*, 1558–1565.
9. Becerril, H. A.; Mao, J.; Liu, Z.; Stoltenberg, R. M.; Bao, Z.; Chen, Y. Evaluation of Solution-Processed Reduced Graphene Oxide Films as Transparent Conductors. *ACS Nano* **2008**, *2*, 463–470.
10. Li, X.; Zhang, G.; Bai, X.; Sun, X.; Wang, X.; Wang, E.; Dai, H. Highly Conducting Graphene Sheets and Langmuir-Blodgett Films. *Nat. Nanotechnol.* **2008**, *3*, 538–542.
11. Lee, J. H.; Shin, D. W.; Makotchenko, V. G.; Nazarov, A. S.; Fedorov, V. E.; Kim, Y. H.; Choi, J.-Y.; Kim, J. M.; Yoo, J.-B. One-Step Exfoliation Synthesis of Easily Soluble Graphite and Transparent Conducting Graphene Sheets. *Adv. Mater.* **2009**, *21*, 4383–4387.
12. Shih, C.; Vijayaraghavan, A.; Krishnan, R.; Sharma, R.; Han, J. H.; Ham, M. H.; Jin, Z.; Lin, S.; Paulus, G. L. C.; Reuel, N. F.; *et al.* Bi-and Trilayer Graphene Solutions. *Nat. Nanotechnol.* **2011**, *6*, 439–445.
13. Li, X.; Wang, X.; Zhang, L.; Lee, S.; Dai, H. Chemically Derived, Ultrasmooth Graphene Nanoribbon Semiconductors. *Science* **2008**, *319*, 1229–1232.
14. Kosynkin, D. V.; Higginbotham, A. L.; Sinitskii, A.; Lomeda, J. R.; Dimiev, A.; Price, B. K.; Tour, J. M. Longitudinal Unzipping of Carbon Nanotubes to Form Graphene Nanoribbons. *Nature* **2009**, *458*, 872–876.
15. Jiao, L.; Wang, X.; Diankov, G.; Wang, H.; Dai, H. Facile Synthesis of High-Quality Graphene Nanoribbons. *Nat. Nanotechnol.* **2010**, *5*, 321–325.
16. Wang, J.; Ma, L.; Yuan, Q.; Zhu, L.; Ding, F. Transition-Metal-Catalyzed Unzipping of Single-Walled Carbon Nanotubes into Narrow Graphene Nanoribbons at Low Temperature. *Angew. Chem., Int. Ed.* **2011**, *50*, 1–6.
17. Cano-Márquez, A. G.; Rodríguez-Macías, F. J.; Campos-Delgado, J.; Espinosa-González, C. G.; Tristán-López, F.; Ramírez-González, D.; Cullen, D. a; Smith, D. J.; Terrones, M.; Vega-Cantú, Y. I. Ex-MWNTs: Graphene Sheets and Ribbons Produced by Lithium Intercalation and Exfoliation of Carbon Nanotubes. *Nano Lett.* **2009**, *9*, 1527–1533.
18. Kosynkin, D. V.; Lu, W.; Sinitskii, A.; Pera, G.; Sun, Z.; Tour, J. M. Highly Conductive Graphene Nanoribbons by Longitudinal Splitting of Carbon Nanotubes Using Potassium Vapor. *ACS Nano* **2011**, *5*, 968–974.
19. Zhu, Y.; Sun, Z.; Yan, Z.; Jin, Z.; Tour, J. M. Rational Design of Hybrid Graphene Films for High-Performance Transparent Electrodes. *ACS Nano* **2011**, *5*, 6472–6479.
20. Ericson, L. M.; Fan, H.; Peng, H.; Davis, V. A; Zhou, W.; Sulpizio, J.; Wang, Y.; Booker, R.; Vavro, J.; Guthy, C.; *et al*. Macroscopic, Neat, Single-Walled Carbon Nanotube Fibers. *Science* **2004**, *305*, 1447–1450.
21. Stankovich, S.; Dikin, D. A.; Dommett, G. H. B.; Kohlhaas, K. M.; Zimney, E. J.; Stach, E. A.; Piner, R. D.; Nguyen, S. T.; Ruoff, R. S. Graphene-Based Composite Materials. *Nature* **2006**, *442*, 282–286.
22. Dimiev, A.; Lu, W.; Zeller, K.; Crowgey, B.; Kempel, L. C.; Tour, J. M. Low-Loss, High-Permittivity Composites Made from Graphene Nanoribbons. *ACS App. Mater. Interfaces* **2011**, *3*, 4657–4661.
23. Harvey, R. G. *Polycyclic Aromatic Hydrocarbons*; Wiley-VCH, Inc.: New York, 1997; p 667.
24. Dresselhaus, M. S.; Dresselhaus, G. Intercalation Compounds of Graphite. *Adv. Phys.* **2002**, *51*, 1–186.
25. Englert, J. M.; Dotzer, C.; Yang, G.; Schmid, M.; Papp, C.; Gottfried, J. M.; Steinruck, H.-P.; Spiecker, E.; Hauke, F.; Hirsch, A. Covalent Bulk Functionalization of Graphene. *Nat. Chem.* **2011**, *3*, 279–286.
26. American Institute of Physics. *American Institute of Physics Handbook*; McGraw-Hill, 1972.
27. Ebbesen, T. W.; Lezec, H. J.; Hiura, H.; Bennett, J. W.; Ghaemi, H. F.; Thio, T. Electrical Conductivity of Individual Carbon Nanotubes. *Nature* **1996**, *382*, 54–56.
28. Jiao, L.; Zhang, L.; Wang, X.; Diankov, G.; Dai, H. Narrow Graphene Nanoribbons from Carbon Nanotubes. *Nature* **2009**, *458*, 877–880.
29. Sun, Y.; Mukherjee, A.; Kuznetsov, O.; Thaner, R.; Alemany, L. B.; Billups, W. E. Functionalization by Reductive Alkylation and Mapping of a Subbituminous Coal by Energy Dispersive X-ray Spectroscopy. *Energy Fuels* **2011**, *25*, 1571–1577.
30. Jiang, Y. J.; Solum, M. S.; Pugmire, R. J.; Grant, D. M.; Schobert, H. H.; Pappano, P. J A New Method for Measuring the Graphite Content of Anthracite Coals and Soots. *Energy Fuels* **2002**, *16*, 1296–1300.
31. Pugmire, R. J.; Solum, M. S.; Jiang, J.; Sarofim, A. F.; Veranth, J.; Schobert, H. H.; Pappano, P. J. The Study of Soot Formation by Solid State NMR Spectroscopy. *Prepr. Symp.-Am. Chem. Soc., Div. Fuel Chem.* **2002**, *47*, 733–735.
32. Gao, W.; Alemany, L. B.; Ci, L.; Ajayan, P. M. New Insights into the Structure and Reduction of Graphite Oxide. *Nat. Chem.* **2009**, *1*, 403–408.
33. Sun, Y.; Kuznetsov, O.; Alemany, L. B.; Billups, W. E. Reductive Alkylation of Anthracite: Edge Functionalization. *Energy Fuels* **2011**, *25*, 3997–4005.
34. Levin, R. H.; Roberts, J. D. Nuclear Magnetic Resonance Spectroscopy. Ring-Current Effects Upon Carbon-13 Chemical Shifts. *Tetrahedron Lett.* **1973**, *14*, 135–138.
35. Bodwell, G. J.; Bridson, J. N.; Cyrański, M. K.; Kennedy, J. W. J.; Krygowski, T. M.; Mannion, M. R.; Miller, D. O. Nonplanar Aromatic Compounds. 8.1 Synthesis, Crystal Structures, and Aromaticity Investigations of the 1, *n*-Dioxa[*n*](2,7)pyrenophanes. How Does Bending Affect the Cyclic π-Electron Delocalization of the Pyrene System? *J Org. Chem.* **2003**, *68*, 2089–2098.
36. Eklund, P. C.; Mahan, G. D.; Spolar, J. G.; Zhang, J. M.; Arakawa, E. T.; Hoffman, D. M. Resonant Raman Scattering in Metals at the Interband Absorption Threshold. *Phys. Rev. B* **1988**, *37*, 691.
37. Jung, N.; Crowther, A. C.; Kim, N.; Kim, P.; Brus, L. Raman Enhancement on Graphene: Adsorbed and Intercalated Molecular Species. *ACS Nano* **2010**, *4*, 7005–7013.
38. Hayashi, S.; Hayamizu, K. Chemical Shift Standards in High-Resolution Solid-State NMR (I) ^{13}C, ^{29}Si, and ^{1}H Nuclei. *Bull. Chem. Soc. Jpn.* **1991**, *64*, 685–687.